A. Mannocchi, C. Giordano, F. Topputo
An Indirect Formulation of Operational Compliant Low-Thrust Trajectories
in: AIAA Scitech 2024 Forum, AIAA, 2024, ISBN: 9781624107115, p. 1-11, AIAA 2024-0631
[AIAA Scitech 2024 Forum, Orlando, FL, USA, 8-12 Jan. 2024]
doi:10.2514/6.2024-0631

An Indirect Formulation of Operational Compliant Low-thrust Trajectories

Alessandra Mannocchi, *, Carmine Giordano, †, and Francesco Topputo ‡
Politecnico di Milano, Via La Masa 34, Milan, 20156, Italy

Deep-space missions will be performed in the future by several stand-alone CubeSats. For limited budget reasons, these spacecraft need to follow operational compliant trajectories: transfers with an alternation of coasting and thrusting periods imposed at pre-defined time instants, the duty cycles. Traditional trajectory optimization algorithms exhibit convergence problems when handling this kind of discontinuous constraints. In this work, an efficient and robust indirect method to compute operational compliant trajectories is formulated through the imposition of coasting arcs as interior-point constraints. Results show that the computed trajectories are similar to the optimal ones with no operational constraint, both in terms of thrusting profile and propellant mass.

I. Introduction

In the last few years, we have been witnessing a significant reduction in space mission costs. An expression of this trend is the rapid development of CubeSat technology [1]. Several released-in-situ, deep-space CubeSat missions are expected to be launched in the next years by ESA (e.g., LUMIO [2], Milani [3], Juventas [4]). Similarly, deep-space stand-alone interplanetary CubeSats, able to travel to their final destination without the need of a carrying mothership, are expected to soon permeate the inner Solar System. The Miniaturised Asteroid Remote Geophysical Observer (M-ARGO) [5] will be the first European CubeSat to perform a similar mission towards a near-Earth asteroid (NEA).

High specific impulse values make electric propulsion a good candidate for this kind of probe [6]. Still, electric propulsion requires a significant effort from on-ground flight dynamics, with regularly scheduled navigation and guidance operations. This is particularly true for stand-alone deep-space CubeSats that, with stringent thrusting, power, and pointing budgets [7], are unable to perform operations, such as communication, ground-based orbit determination and correction, or scientific experiments, while thrusting. To overcome these issues CubeSats will be required to follow operational-compliant (OC) trajectories, consisting of a repetition of a regular pattern of alternating thrusting and coasting arcs (duty cycles). OC trajectories can be designed in any way necessary to ease ground operations, for example miming the working week (e.g., 7 days duty cycles, with 6 days of thrust and 1 day of coasting).

Electric propulsion trajectories are designed by formulating a low-thrust optimal trajectory problem (LOTP) [8, 9]. No analytic solutions exist for this problem, but several numerical techniques, traditionally divided into direct and indirect methods [10], have been developed to solve it. In this work we focus on the indirect formulation [11, 12], aiming at finding the solution of the necessary optimality conditions derived by calculus of variations. The solutions of an indirect formulation are computed through some sort of gradient methods [13, 14], leveraging on the first, and sometimes second, order derivatives of the problem, thus required to be differentiable at least up to the first order.

Duty cycles are time-dependent and discontinuous constraints, and for this reason not straightforward to introduce in indirect methods [15]. Their presence is usually ignored in the preliminary trajectory design phases. Homotopy technique, or continuation, is a class of methods conceived to deal with discontinuous structures in the LOTP. They allow the solution of the original, difficult, and discontinuous problem, starting from an easier one [16]. It is usually employed in indirect methods to overcome discontinuity problems as bang-bang control in fuel optimal solutions [17, 18], to impose varying maximum thrust models [19] and shutdown of the thruster due to eclipses [20]. Recently, the problem of forced coasting arcs imposition has become more and more relevant, and homotopic techniques have been employed to solve it [21, 22] also in direct formulations [23].

In this work, an alternative formulation based on the modeling of the alternation of duty cycles as interior-point constraints is proposed. The solution method relies on the use of analytical derivatives, switching times detection techniques, as well as a pre-computation of them, and a triple continuation scheme rapidly generating OC low-thrust

*PhD Student, Department of Aerospace Science and Technology (DAER). AIAA student member.
†PostDoc Fellow, Department of Aerospace Science and Technology (DAER). AIAA member.
‡Full Professor, Department of Aerospace Science and Technology (DAER). AIAA senior member.

trajectories. The main contribution of the work is the presentation of a simple method capable of modeling duty cycles with duration of any kind without any prior knowledge of the structure of the control law. The formulation is used to solve fuel optimal trajectories in M-ARGO CubeSats scenario, and is shown to compute OC trajectories with thrusting profiles, and required propellant mass, similar to the solutions without the duty cycle imposition, and thus nearly optimal.

II. Problem Statement

A. Shooting Problem

The equations of the dynamics of a spacecraft in cartesian coordinates in an interplanetary two-body problem are

$$\dot{\mathbf{x}} = \mathbf{f}(\mathbf{x}, \boldsymbol{\alpha}, u) \Rightarrow \begin{cases} \dot{\mathbf{r}} = \mathbf{v} \\ \dot{\mathbf{v}} = -\frac{\mu}{r^3}\mathbf{r} + u\frac{T_{max}}{m}\boldsymbol{\alpha} \\ \dot{m} = -u\frac{T_{max}}{I_{sp}g_0} \end{cases} \tag{1}$$

where $\mathbf{r}$, $\mathbf{v}$ and m are respectively the spacecraft position, velocity, and mass, and r is the norm of the position vector. The control is provided by the vector $\boldsymbol{\alpha}$, the thrust direction unit vector, and $u \in [0, 1]$, the thrust throttle factor. The values μ, g_0, I_{sp}, and T_{max} are the gravitational constant of the Sun, the Earth gravitational acceleration at sea level, the specific impulse and the maximum thrust, respectively. The LOTP aims at computing the optimal controls $\boldsymbol{\alpha}^*$ and u^* that minimizes J, a scalar cost function, under some boundary conditions at the initial and final times, t_i and t_f. If the objective is to save the propellant mass m_p, the LOTP is called a fuel-optimal (FO) problem, and the cost function is

$$J_f = \frac{T_{max}}{I_{sp}} \int_{t_i}^{t_f} u \, \mathrm{d}t \tag{2}$$

while the boundary conditions are expressed as

$$\mathbf{r}(t_i) = \mathbf{r}_i; \quad \mathbf{v}(t_i) = \mathbf{v}_i \quad \text{and} \quad m(t_i) = m_i \tag{3}$$

$$\mathbf{r}(t_f) = \mathbf{r}_T(t_f) \quad \text{and} \quad \mathbf{v}(t_f) = \mathbf{v}_T(t_f) \tag{4}$$

where $\mathbf{r}_T(t_f)$ and $\mathbf{v}_T(t_f)$ are the known position and velocity of the target at the final time. The indirect formulation of the problem aims at finding a solution to the necessary conditions for optimality, which are derived by introducing the Lagrange multipliers, or costates, $\boldsymbol{\lambda} = [\boldsymbol{\lambda}_r, \boldsymbol{\lambda}_v, \lambda_m]$ associated to the states. Considering the Hamiltonian function

$$H_f = J_f + \boldsymbol{\lambda}^T \cdot \mathbf{f} = \boldsymbol{\lambda}_r \cdot \mathbf{v} + \boldsymbol{\lambda}_v \cdot \left(-\frac{\mu}{r^3}\mathbf{r} + u\frac{T_{max}}{m}\boldsymbol{\alpha}\right) + \lambda_m\left(-u\frac{T_{max}}{I_{sp}g_0}\right) + u\frac{T_{max}}{I_{sp}g_0} \tag{5}$$

It can be proved [24, 25] that the optimal thrust direction $\boldsymbol{\alpha}^*$ is such that H is minimized at any time instant by virtue of the Pontryagin minimum principle (PMP), i.e.,

$$\boldsymbol{\alpha}^* = -\frac{\boldsymbol{\lambda}_v}{\lambda_v} \quad \text{if} \quad \lambda_v \neq 0 \tag{6}$$

where λ_v is the norm of $\boldsymbol{\lambda}_v$, while the optimal thrust throttle factor u^* is

$$u^* = \begin{cases} 0 & \text{if} \quad S_f > 0 \\ \in [0, 1] & \text{if} \quad S_f = 0 \\ 1 & \text{if} \quad S_f < 0 \end{cases} \tag{7}$$

where S_f is the optimal switching function, $S_f = 1 - \lambda_m - \lambda_v\frac{I_{sp}g_0}{m}$. Accordingly to Eq. (7), the control exhibits a bang-bang, discontinuous profile [8]. Homotopy technique was introduced in [17] to smooth the control profile, and gradually introduce the discontinuity into the problem. The idea was to start solving an easier problem, the energy optimal (EO) one, having the following objective function

$$J_\epsilon = \frac{T_{max}}{I_{sp}} \int_{t_i}^{t_f} [u - \epsilon u(1-u)] \, \mathrm{d}t \tag{8}$$

with the parameter $\epsilon = 1$. The problem is solved iteratively gradually reducing ϵ and providing as an initial guess the solution to the previous problem until $\epsilon = 0$, which corresponds to the solution of the FO problem. The Hamiltonian of these auxiliary problems reads

$$H_\epsilon = J_\epsilon + \boldsymbol{\lambda}^T \cdot \mathbf{f} = \boldsymbol{\lambda}_r \cdot \mathbf{v} - \frac{\mu}{r^3} \mathbf{r} \cdot \boldsymbol{\lambda}_v + u \frac{T_{max}}{I_{sp} g_0} (S_\epsilon - \epsilon + \epsilon u) \tag{9}$$

where S_ϵ is the switching function for the EO, and $S_\epsilon = S_f$. Applying the PMP to the auxiliary problem, it can be proved that the optimal thrust direction $\boldsymbol{\alpha}^*$ is the same as Eq. (6), while the optimal thrust throttle factor u^* is

$$u^* = \begin{cases} 0 & \text{if} \quad S_\epsilon > \epsilon \\ \frac{\epsilon - S_\epsilon}{2\epsilon} & \text{if} \quad |S_\epsilon| \leq \epsilon \\ 1 & \text{if} \quad S_\epsilon < -\epsilon \end{cases} \tag{10}$$

As $\boldsymbol{\alpha}^*$ and u^* depend on the state and costate $\mathbf{y} = [\mathbf{x}, \, \boldsymbol{\lambda}]$, to find the optimal control they have to be integrated for the whole trajectory, with the following augmented equations of the dynamics

$$\dot{\mathbf{y}} = \mathbf{F}(\mathbf{y}) \Rightarrow \begin{cases} \dot{\mathbf{r}} = \mathbf{v} \\ \dot{\mathbf{v}} = -\frac{\mu}{r^3} \mathbf{r} + u \frac{T_{max}}{m} \boldsymbol{\alpha} \\ \dot{m} = -u \frac{T_{max}}{I_{sp} g_0} \\ \dot{\boldsymbol{\lambda}}_r = -\frac{3\mu}{r^5} (\mathbf{r} \cdot \boldsymbol{\lambda}_v) \mathbf{r} + \frac{\mu}{r^3} \boldsymbol{\lambda}_v \\ \dot{\boldsymbol{\lambda}}_v = -\boldsymbol{\lambda}_r \\ \dot{\lambda}_m = -\frac{u \lambda_v T_{max}}{m^2} \end{cases} \tag{11}$$

Enforcing the boundary conditions Eqs. (3, 4) at t_i and t_f, plus the condition $\lambda_m(t_f) = 0$, since no final condition is enforced on the mass [8]. Thus, being $\mathbf{y}(t) = \boldsymbol{\varphi}_\epsilon(\mathbf{y}_i, t_i, t)$ the solution flow for a specific ϵ value of Eq. (11) integrated from the initial time t_i to a generic time instant t, and with $\boldsymbol{\alpha}^*$ and u^* provided by Eq. (6) and Eq. (10), respectively, the EO and FO shooting problems aim to find λ_i^* such that $\mathbf{y}(t_f) = \boldsymbol{\varphi}_\epsilon([\mathbf{x}_i, \, \lambda_i^*], t_i, t_f)$ satisfies the boundary conditions

$$\begin{bmatrix} \mathbf{r}(t_f) - \mathbf{r}_T(t_f) \\ \mathbf{v}(t_f) - \mathbf{v}_T(t_f) \\ \lambda_m(t_f) \end{bmatrix} = \mathbf{0} \tag{12}$$

B. Duty Cycle Constraint

In OC trajectory design the objective is to switch off the engine according to the duty cycle scheme to impose. In order to satisfy the necessary conditions of optimality, this event will be treated in this work as an interior-point constraint [8]. We define $S_{DC} = S_{DC}(t)$ the duty cycle switching function, depending only on time, and we properly model it to impose that the engine switches off every time the function crosses a certain value ϵ_{DC} (see Subsec. IV.A). Accordingly, the optimal throttle factor in Eq. (10) turns into

$$u^* = \begin{cases} 0 & \text{if} \quad S_\epsilon > \epsilon \quad \text{or} \quad S_{DC} < \epsilon_{DC} \\ \frac{\epsilon - S_\epsilon}{2\epsilon} & \text{if} \quad |S_\epsilon| \leq \epsilon \quad \text{and} \quad S_{DC} \geq \epsilon_{DC} \\ 1 & \text{if} \quad S_\epsilon < -\epsilon \quad \text{and} \quad S_{DC} \geq \epsilon_{DC} \end{cases} \tag{13}$$

Supposing that S_DC crosses ϵ_{DC} at a certain switching time instant t_s. Then, the following jump necessary conditions have to be satisfied [8]

$$H(t_s^-) = H(t_s^+) - \pi \left. \frac{\partial S_{DC}}{\partial t} \right|_{t_s} \tag{14}$$

$$\boldsymbol{\lambda}(t_s^-) = \boldsymbol{\lambda}(t_s^+) + \pi \left.\frac{\partial S_{DC}}{\partial \mathbf{x}}\right|_{t_s} \tag{15}$$

where π is a scalar Lagrange multiplier. In particular, evaluating the Hamiltonian at t_s^- and t_s^+ with Eq. (9), noting that $S_\epsilon(t_s^-) = S_\epsilon(t_s^+) = S_\epsilon(t_s)$, and plugging this information into Eq. (14), a closed form of π can be computed as

$$\pi = \left(\left.\frac{\partial S_{DC}}{\partial t}\right|_{t_s} \right)^{-1} \frac{T_{max}}{I_{sp} g_0} [\Delta u (S_\epsilon(t_s) - \epsilon) + \epsilon (u(t_s^-)^2 - u(t_s^+)^2)] \tag{16}$$

where $\Delta u = u(t_s^-) - u(t_s^+)$. As S_{DC} depends only on time, the only discontinuity is in the Hamiltonian function, while the costates remain continuous across ϵ_{DC}. This fact, in addition to the existence of a closed form of π given by Eq. (16), transforms a potential tedious multi-point boundary value problem generated by the interior-point constraints [26] into a simpler two-point boundary value problem. Accordingly, no other discontinuities are introduced in the integration of Eq. (11) when solving the EO and FO shooting problems.

III. Solution Method

A. Analytical Derivatives

To increase the accuracy and robustness of the computation, analytic derivatives of the shooting problem are computed. In particular from Eq. (11) the state transition matrix (STM) $\boldsymbol{\Phi}(t_i, t)$ is derived. The STM maps small variations in the initial conditions $\partial \mathbf{y}_i$ over a generic time instant $t > t_i$, i.e., $\partial \mathbf{y}(t) = \boldsymbol{\Phi}(t_i, t) \partial \mathbf{y}(t_i)$. The STM is subjected to the variational equation

$$\dot{\boldsymbol{\Phi}}(t, t_i) = D_y \mathbf{F} \boldsymbol{\Phi}(t, t_i) \quad \text{with} \quad \boldsymbol{\Phi}(t_i, t_i) = \mathbf{I}_{14x14} \tag{17}$$

where $D_y\mathbf{F}$ is the Jacobian matrix of $\mathbf{F}(\mathbf{y})$, and has has two different expressions based on whether u^* is constant. Being subject to a variational equation, $\boldsymbol{\Phi}(t_i, t)$ has to be integrated with states and costates. Defining as $\mathbf{z} = [\mathbf{y},\ \mathrm{vec}(\boldsymbol{\Phi})]$ the 210-dimensional vector containing the 14 variables of $\mathbf{y}$ and the 196 elements of $\boldsymbol{\Phi}$, where the 'vec' operator converts a matrix into a vector, the integration to perform to solve the problem is

$$\dot{\mathbf{z}} = \mathbf{G}(\mathbf{z}) \Rightarrow \begin{cases} \dot{\mathbf{y}} = \mathbf{F}(\mathbf{y}) \\ \mathrm{vec}(\dot{\boldsymbol{\Phi}}) = \mathrm{vec}(D_y \mathbf{F} \boldsymbol{\Phi}) \end{cases} \tag{18}$$

However, $\boldsymbol{\Phi}$ maps states and costates along a continuous trajectory, but the bang-bang profile given by Eq. (13) creates discontinuities in it. At each switching time t_s, compensations in the STM $\boldsymbol{\Psi}(t_s)$ have to be added using the chain rule [27]

$$\boldsymbol{\Phi}(t_f, t_i) = \boldsymbol{\Phi}(t_f, t_N^+) \boldsymbol{\Psi}(t_N) \boldsymbol{\Phi}(t_N^-, t_{N-1}^+) \boldsymbol{\Psi}(t_{N-1}) \dots \boldsymbol{\Phi}(t_2^-, t_1^+) \boldsymbol{\Psi}(t_1) \boldsymbol{\Phi}(t_1^-, t_i) \tag{19}$$

where N is the total number of discontinuities. Suppose that the discontinuity is detected at t_s for the switching function S_f crossing 0, and thus for the optimal control u^* jumping from 0 to 1 or vice versa. In this case $\mathbf{y}$ is continuous, but $\dot{\mathbf{y}}$ is discontinuous, and it can be proved [19] that the compensation matrix $\boldsymbol{\Psi}_f(t_s)$ is given by

$$\boldsymbol{\Psi}_f(t_s) = \frac{\partial \mathbf{y}(t_s^+)}{\partial \mathbf{y}(t_s^-)} = \mathbf{I}_{14x14} + (\dot{\mathbf{y}}(t_s^+) - \dot{\mathbf{y}}(t_s^-)) \frac{1}{\dot{S}_f} \frac{\partial S_f}{\partial \mathbf{y}} \tag{20}$$

where $\dot{S}_f$ is the time derivative of the optimal switching function. Suppose instead that the jump for u^* from 0 to 1 or vice versa at t_s is due to the switching function S_{DC} crossing ϵ_{DC}. Also in this case $\mathbf{y}$ is continuous and $\dot{\mathbf{y}}$ is discontinuous, but no compensation matrix is needed. Indeed, since $\partial S_{DC} / \partial \mathbf{y} = \mathbf{0}$, it results that

$$\boldsymbol{\Psi}_{DC}(t_s) = \frac{\partial \mathbf{y}(t_s^+)}{\partial \mathbf{y}(t_s^-)} = \mathbf{I}_{14x14} \tag{21}$$

Indeed $\boldsymbol{\Psi}(t_s)$ maps variations of $\mathbf{y}(t_s^-)$ in variations in $\mathbf{y}(t_s^+)$, and S_{DC} does not depends on the $\mathbf{y}$, but only on time. Therefore, during the integration of Eq. (18), no corrections to the STM are necessary for switching in S_{DC}.

B. Switching Detection Technique

During the integration of Eq. (18) the detection of the switching time t_s is essential because discontinuities cause accumulation of the integration error around those instants, and because it is necessary to introduce the compensation matrices $\mathbf{\Psi}(t_s)$ through Eq. (20). However, no prior information on the structure of the thrusting profile is known. Let t_k and t_{k+1} be two consecutive integration time instant, and $\mathbf{y}_k$ and $\mathbf{y}_{k+1}$ the correspondent states and costates. If, e.g., $(S_\epsilon(\mathbf{y}_k) - \epsilon)(S_\epsilon(\mathbf{y}_{k+1}) - \epsilon)) < 0$, there exists $t_s \in [t_k, t_{k+1}]$ such that $S_\epsilon(t_s) = \epsilon$. Then, the switching detection technique implemented in [28] with tolerance 10^{-12} is implemented to detect t_s. This technique is employed in every switching of the S_ϵ function.

As regards the S_{DC} function, even if no compensation matrix is necessary for the crossing of ϵ_{DC}, the identification of the time instants when this happens is necessary for the accuracy of the integration. However, being S_{DC} function only of time, and being the final time t_f fixed in the considered problem, its switching time instants t_s can be identified regardless of the integration. For this reason, in this work, they are pre-computed and then enforced in the integration.

C. Triple Continuation Scheme

The discontinuities introduced by the S_{DC} prevent the solver to reach convergence. This is particularly true as the number of coasting arcs to be imposed increases and their duration decreases. For this reason, a triple continuation scheme based on the eclipses imposition in [20] is implemented here. The approach called N_{max} continuation, gradually turns inactive coasting arcs into active ones, i.e., the maximum number of forced coasting arcs N_{max} increases at each iteration of the continuation scheme. For a better convergence of the algorithm, both this continuation and the one on ϵ to solve a FO problem starting from an EO one, are employed.

The starting point of the continuation scheme requires the solution of the EO problem without the duty cycles imposition. Then, the FO solution is computed gradually decreasing $\epsilon : 1 \rightarrow 0$. Only then the N_{max} continuation is employed to gradually enforce the coasting arcs. This combination is used, and not the other way round, i.e., first the N_{max} continuation and then the ϵ continuation, because in this way an ill-conditioned STM preventing the convergence would be encountered only at the final steps of the integration.

The N_{max} continuation is depicted in Fig. 1. The variable u_ζ is defined as the throttle factor in the N_{max}-th coasting arc to be imposed, and it is the third parameter on which a continuation is performed. Starting from the FO solution (i.e., $N_{max} = 0$ and $u_\zeta = 0$), the number of active coasting arcs N_{max} is increased from 0 to 1. The FO solution is used as the initial guess for this auxiliary problem (i.e., $N_{max} = 1$ and $u_\zeta = 0$). Supposing the solution of this problem is obtained, N_{max} is increased from 1 to 2, and the new auxiliary problem is solved (i.e., $N_{max} = 2$ and $u_\zeta = 0$). Suppose that instead, in this case, the solver fails. Then, the problem u_ζ is imposed as 1, and the new problem is solved (i.e., $N_{max} = 2$ and $u_\zeta = 1$). The value of u_ζ is gradually reduced until $u_\zeta = 0$ is obtained. Starting from this solution as an initial guess, a new problem with $N_{max} = 3$ and $u_\zeta = 0$ is solved, and so on until the trajectory is OC.

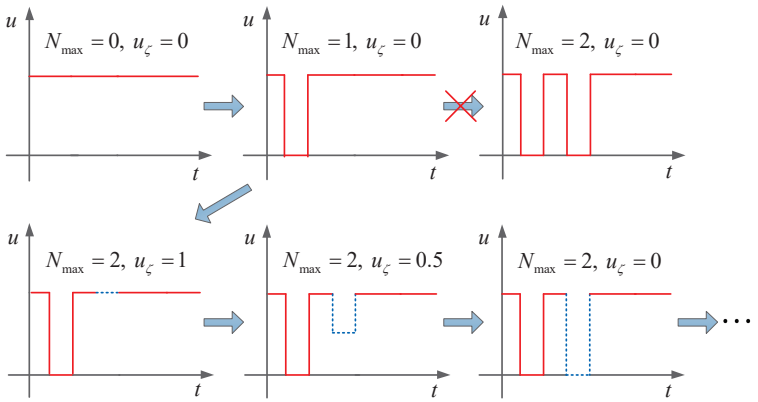

Fig. 1 N_{max} continuation scheme.

Since the third continuation is on the gradual reduction of u_ζ to 0, the minimum value of the throttle factor u_{min} in the N_{max}-th forced coasting arc is not always 0. In particular, accordingly to the PMP [20], the optimal throttle factor turns into Eq. (13) to

$$u^* = \begin{cases} u_{min} & \text{if} \quad S_\epsilon > (1-2u_{min})\epsilon & \text{or} \quad S_{DC} < \epsilon_{DC} \\ \frac{\epsilon - S_\epsilon}{2\epsilon} & \text{if} \quad -\epsilon \le S_\epsilon \le (1-2u_{min})\epsilon & \text{and} \quad S_{DC} \ge \epsilon_{DC} \\ 1 & \text{if} \quad S_\epsilon < -\epsilon & \text{and} \quad S_{DC} \ge \epsilon_{DC} \end{cases} \tag{22}$$

where u_{min} is $u_\zeta = 1 \rightarrow 0$ in the N_{max}-the forced coasting arc, and 0 otherwise.

IV. Results

A. Duty Cycle Switching Function Modeling

The duty cycle switching function $S_{DC} = S_{DC}(t)$, depending only on time, has to be properly modeled to impose the OC trajectory shape required, i.e., the correct duration of each forced coasting arc. This is performed by requiring that the engine switches off every time the function crosses a certain value ϵ_{DC}. To model the $S_{DC}(t)$, a pulse wave function is selected. In particular, due to its regularity and smoothness with respect to the normal pulse wave function, an expansion based on the sinc function $\text{sinc}(t) = \sin(\pi t)/\pi t$ is employed as

$$S_{DC}(t) = \frac{A\tau}{T}\left(1 + 2\sum_{n=1}^{\infty}(\text{sinc}(n\frac{\tau}{T})\cos(2\pi n f t))\right) \tag{23}$$

where A is the amplitude, T is the period, τ is the pulse length, and $f = 1/T$ is the frequency, of the pulse wave. These values are customized in order to enforce the right duration of the coasting arcs, e.g., to have duty cycles corresponding to a working week with 6 days of thrusting and 1 day of coasting, T is imposed to be 7 days, and τ to be 6 days (see Fig. 2(a) for reference). The expansion of the wave is truncated at a value n significantly high in order to have a smoothness in the function. To avoid the peaks due to the Gibbs phenomenon in the sinc function expansion (see Fig. 2(b)) ϵ_{DC} is set to be half the value of the amplitude A, and the pulse wave expansion has been truncated at $n = 30$, in this way the phenomenon does not create disturbances in the integration. In all the simulations in Subsec. IV.B the values of the sinc function parameters have been modified to model different duration of the duty cycles: A has been imposed 0.2, and thus $\epsilon_{DC} = 0.1$. The values of T and τ have been varied to model different duration of the duty cycles.

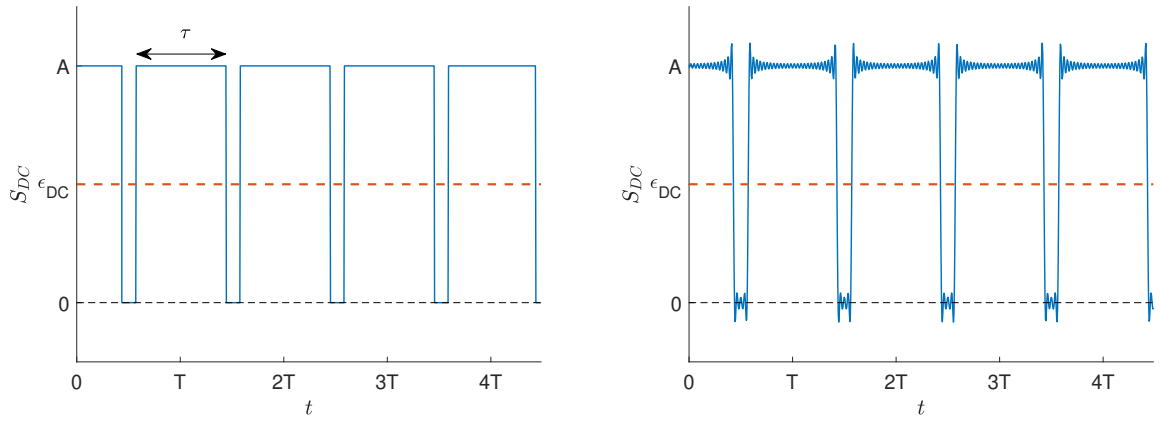

(a) *Pulse wave modeling the duty cycles alternation.*

(b) *Pulse wave modeling with sinc expansion.*

Fig. 2 Duty cycle switching function modeling as a pulse wave.

B. Numerical Simulations

The simulations in this subsection have been solved with a normalization of the variables involved with the constants listed in Table 1. The simulations have been performed with an Intel i9-9980HK, a total RAM of 16 GB, and Matlab R2022b. To perform the continuation in ϵ, it has been imposed a variation $\Delta\epsilon = 0.05$, while for u_ζ a variation $\Delta u_\zeta = 0.1$. At each iteration, slightly increased values of the variations are used if the solver converges, i.e., $\Delta\epsilon_{new} = 1.01\Delta\epsilon_{old}$ and $\Delta u_{\zeta,new} = 1.01\Delta\, u_{\zeta,old}$, otherwise the variations are halved. The continuations fail if $\Delta u_\zeta < 0.005$ or $\Delta\epsilon < 10^{-8}$.

The integration to solve the shooting problems are performed using a variable-step 7^{th}-8^{th} Runge–Kutta integration scheme, where it has been imposed an integration tolerance of 10^{-11} and a maximum integration step in order to have at least 3 nodes into each coasting arc and avoid integration error to accumulate. To find the initial converging guess for the EO problem with $\epsilon = 1$ the Adjoint Control Transformation (ACT) initialization has been employed [27] 20 times to find the first solution of the EO problem, otherwise the algorithm fails.

Parameter	**Value**
Sun gravitational constant, μ	1.327124×10^{11} km^3/s^2
Earth gravitational acceleration, g_0	9.80665 m/s^2
Length unit	1.495978×10^{8} km
Time unit	5.022643×10^{6} s
Velocity unit	29.784692 km/s
Mass unit	28.2 kg
Force unit	0.142322 N

Table 1 Constants used in the normalization.

The scenario to which the shooting problem was applied is the M-ARGO CubeSat one. The assumptions for the simulations are reported in Table 2. The ephemerides of the asteroid 2010 UE51 are retrieved from the Spacecraft Planet Instrument Camera-matrix Events (SPICE) kernels of the HORIZONS system [29]. The departure date is set the 17^{th} September 2023, with a time of flight of 581 days. The CubeSat is supposed to depart from the Sun–Earth L2 Lagrangian point, and to rendez-vou with the asteroid.

Parameter	**Value**
Asteroid	2010 UE51
Departure date	17 September 2023
Time of flight	581 days
T_{max}	1.3 mN
I_{sp}	3500 s
m_0	28.2 kg

Table 2 Scenario assumptions.

The results of the simulations are reported in Table 3. The CPU time required to compute the FO solution in the first row is indicative since it only depends on the ACT initialization. The integration code is converted to MEX to speed up simulations. The increment in propellant mass Δm_p is computed with respect to the m_p of the FO solution of 0.907208 kg. The CPU time to compute the solution increases with the frequency of the duty cycles, i.e., as T decreases, but it is still contained, requiring less than 6 minutes to compute the worst case scenario with $T = 5$ days and $\tau = 4$ days. The trajectories in the J2000 reference frame, as well as the throttle factor u profiles, the optimal switching function S_f, and the duty cycle switching function S_{DC}, are reported in Fig. 3-7. For the trajectories, the red arcs are the thrust ones, while the dashed blue ones are the coasting arcs. For the u and S_f profiles, the green lines highlight the zone where $S_f > 0$. All the OC thrust profiles mimic the shape of the FO solution in Fig. 3(b).

T (days)	$\boldsymbol{\tau}$ (days)	$\mathbf{m_p}$ (kg)	$\mathbf{\Delta\, m_p}$ (%)	**CPU time** (s)
-	-	0.907208	-	28.32
30	25	0.913540	0.6980	5.15
15	10	0.942919	3.9364	11.59
7	6	0.911911	0.5184	72.62
5	4	0.916394	1.0126	87.68

Table 3 Simulations results.

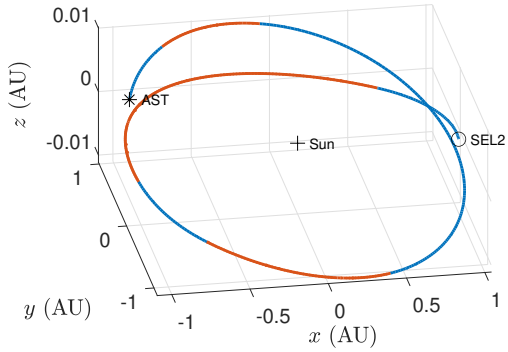

(a) *Trajectory in the J2000 reference frame.*

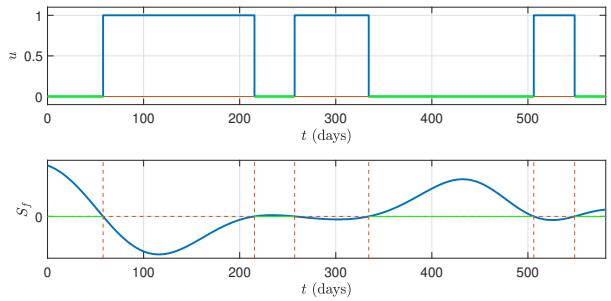

(b) *Throttle factor and optimal switching function profiles.*

Fig. 3 FO solution trajectory.

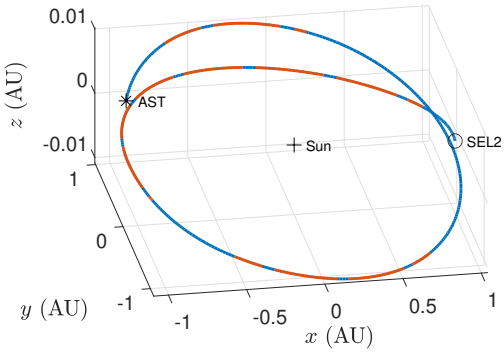

(a) *Trajectory in the J2000 reference frame.*

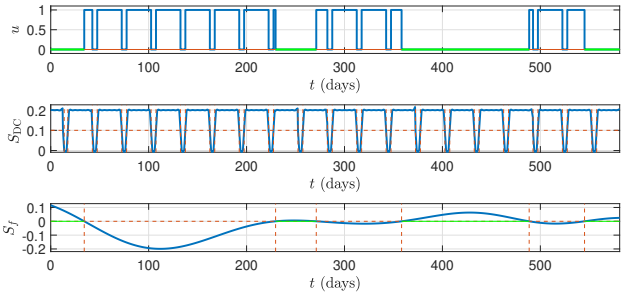

(b) *Throttle factor, optimal switching function, and duty cycle switching function profiles.*

Fig. 4 Solution for $T = 30$ days and $\tau = 25$ days.

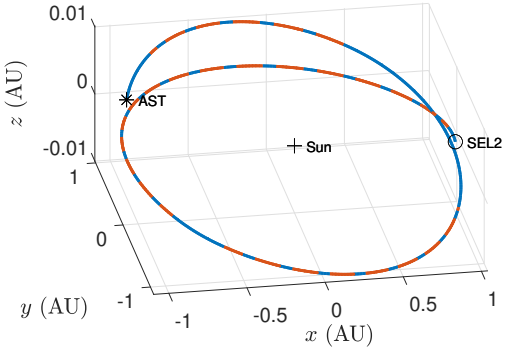

(a) *Trajectory in the J2000 reference frame.*

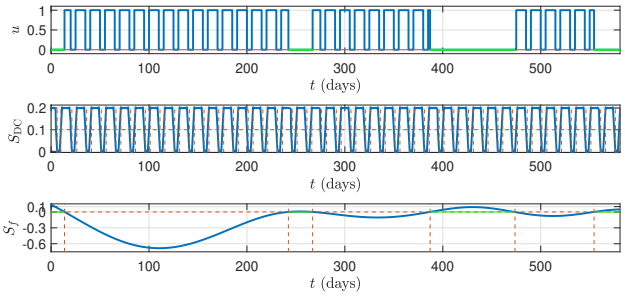

(b) *Throttle factor, optimal switching function, and duty cycle switching function profiles.*

Fig. 5 Solution for $T = 15$ days and $\tau = 10$ days.

V. Conclusion

In this work, the problem of the OC trajectories, trajectories characterized by a pre-defined alternation of thrusting and coasting arcs, is investigated. A novel formulation of the OC constraint in indirect trajectory optimization is presented. The optimization is based on a triple continuation scheme, on the imposition of the forced coast arcs through an interior-point formalization, and the use of analytic derivatives for robustness and accuracy. The necessary conditions

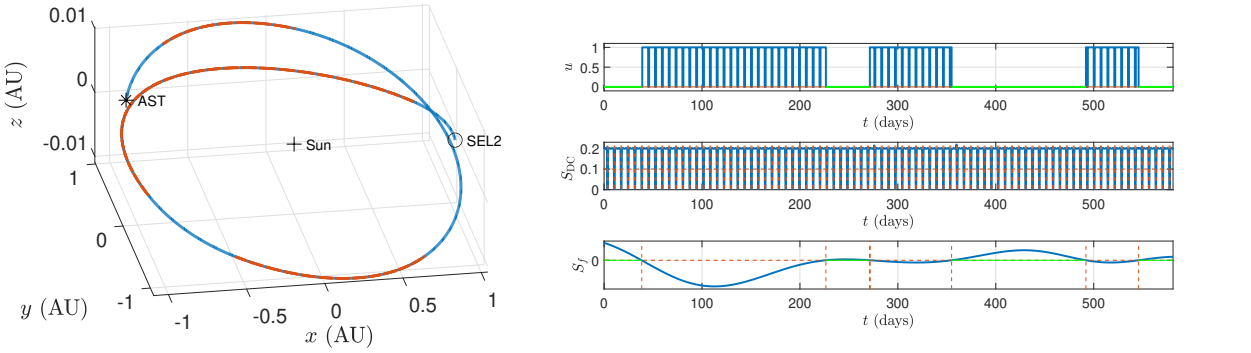

(a) *Trajectory in the J2000 reference frame.* (b) *Throttle factor, optimal switching function, and duty cycle switching function profiles.*

Fig. 6 Solution for $T = 7$ days and $\tau = 6$ days.

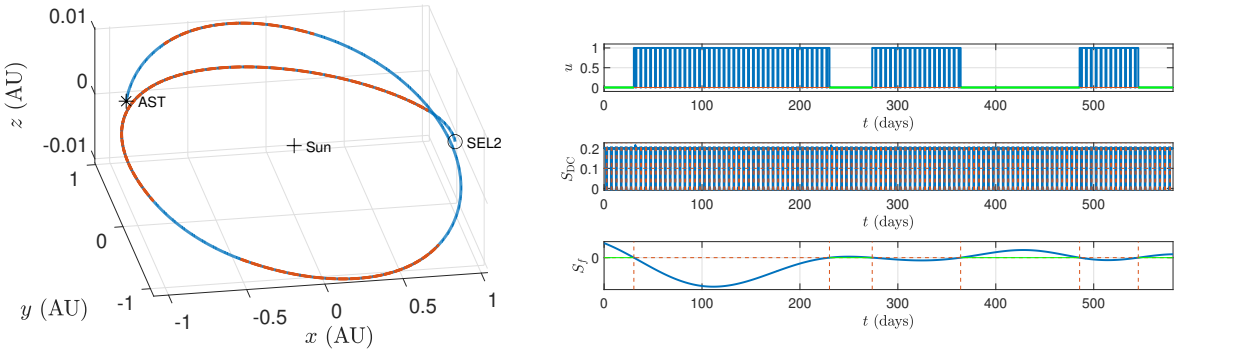

(a) *Trajectory in the J2000 reference frame.* (b) *Throttle factor, optimal switching function, and duty cycle switching function profiles.*

Fig. 7 Solution for $T = 5$ days and $\tau = 4$ days.

for optimality are derived for the fuel optimal problem, as well as the jump conditions in the Hamiltonian, while it is proved that no discontinuities are imposed on the costates and to the STM. The proposed method is applied to M-ARGO CubeSat scenario. Through several tests, it is proven to generate OC trajectories in a fast way, without any need for prior knowledge of the thrust profile. Future work on the method will investigate the possibility of introducing a variable maximum thrust and specific impulse model into the dynamics, as well as the solution to the time-optimal OC problem.

Acknowledgments

This project has received funding from the European Research Council (ERC) under the European Union's Horizon 2020 research and innovation program (grant agreement No. 864697).

A. Mannocchi and F. Topputo would also like to acknowledge the funding received under ESA Contracts No. 4000136010/21/NL/GLC/my.

References

[1] Walker, R., Binns, D., Bramanti, C., Casasco, M., Concari, P., Izzo, D., Feili, D., Fernandez, P., Fernandez, J. G., Hager, P., Koschny, D., Pesquita, V., Wallace, N., Carnelli, I., Khan, M., Scoubeau, M., and Taubert, D., "Deep-space CubeSats: thinking inside the box," *Astronomy & Geophysics*, Vol. 59, No. 5, 2018, pp. 5.24–5.30. https://doi.org/10.1093/astrogeo/aty232.

[2] Cervone, A., Topputo, F., Speretta, S., Menicucci, A., Turan, E., Di Lizia, P., Massari, M., Franzese, V., Giordano, C., Merisio, G., et al., "LUMIO: A CubeSat for observing and characterizing micro-meteoroid impacts on the Lunar far side," *Acta Astronautica*, Vol. 195, 2022, pp. 309–317. https://doi.org/10.1016/j.actaastro.2022.03.032.

[3] Ferrari, F., Franzese, V., Pugliatti, M., Giordano, C., and Topputo, F., "Trajectory options for Hera's Milani CubeSat around (65803) Didymos," *The Journal of the Astronautical Sciences*, Vol. 68, No. 4, 2021, pp. 973–994. https://doi.org/10.1007/s40295-021-00282-z.

[4] Goldberg, H. R., Karatekin, Ö., Ritter, B., Herique, A., Tortora, P., Prioroc, C., Gutierrez, B. G., Martino, P., and Carnelli, I., "The Juventas CubeSat in support of ESA's Hera mission to the asteroid Didymos," *Proceedings of the Small Satellite Conference*, SSC19-WKIV-05, Vol. 1, Utah State University, Logan, UT, 2019.

[5] Topputo, F., Wang, Y., Giordano, C., Franzese, V., Goldberg, H., Perez-Lissi, F., and Walker, R., "Envelop of reachable asteroids by M-ARGO CubeSat," *Advances in Space Research*, Vol. 67, No. 12, 2021, pp. 4193–4221. https://doi.org/10.1016/j.asr.2021.02.031.

[6] Pascoa, J. C., Teixeira, O., and Filipe, G., "A review of propulsion systems for CubeSats," *ASME International Mechanical Engineering Congress and Exposition*, V001T03A039, Vol. 1, Pittsburg, PA, 2018. https://doi.org/10.1115/IMECE2018-88174.

[7] Martin-Mur, T. J., Gustafson, E. D., and Young, B. T., "Interplanetary CubeSat navigational challenges," *25th International Symposium on Space Flight Dynamics (ISSFD)*, Munich, Germany, 2015.

[8] Bryson, A., and Ho, Y.-C., *Applied optimal control*, Taylor & Francis, London, 1975. https://doi.org/10.1201/9781315137667.

[9] Hull, D. G., *Optimal control theory for applications*, Springer Science & Business Media, Berlin, Germany, 2013. https://doi.org/10.1007/978-1-4757-4180-3.

[10] Betts, J. T., "Survey of Numerical Methods for Trajectory Optimization," *Journal of Guidance, Control, and Dynamics*, Vol. 21, No. 2, 1998, pp. 193–207. https://doi.org/10.2514/2.4231.

[11] Kechichian, J. A., "Optimal low-Earth-orbit-geostationary-Earth-orbit intermediate acceleration orbit transfer," *Journal of Guidance, Control, and Dynamics*, Vol. 20, No. 4, 1997, pp. 803–811. https://doi.org/10.2514/2.4116.

[12] Ranieri, C. L., and Ocampo, C. A., "Indirect optimization of three-dimensional finite-burning interplanetary transfers including spiral dynamics," *Journal of Guidance, Control, and Dynamics*, Vol. 32, No. 2, 2009, pp. 445–455. https://doi.org/10.2514/1.38170.

[13] Morante, D., Sanjurjo Rivo, M., and Soler, M., "A survey on low-thrust trajectory optimization approaches," *Aerospace*, Vol. 8, No. 3, 2021, p. 88. https://doi.org/10.3390/aerospace8030088.

[14] Betts, J. T., *Practical methods for optimal control and estimation using nonlinear programming*, SIAM, Philadelphia, PA, 2010. https://doi.org/10.1137/1.9780898718577.

[15] Li, T., Wang, Z., and Zhang, Y., "Double-homotopy technique for fuel optimization of power-limited interplanetary trajectories," *Astrophysics and Space Science*, Vol. 364, No. 9, 2019, pp. 1–12. https://doi.org/10.1007/s10509-019-3637-6.

[16] Jiang, F., Baoyin, H., and Li, J., "Practical techniques for low-thrust trajectory optimization with homotopic approach," *Journal of Guidance, Control, and Dynamics*, Vol. 35, No. 1, 2012, pp. 245–258. https://doi.org/10.2514/1.52476.

[17] Bertrand, R., and Epenoy, R., "New smoothing techniques for solving bang–bang optimal control problems—numerical results and statistical interpretation," *Optimal Control Applications and Methods*, Vol. 23, No. 4, 2002, pp. 171–197. https://doi.org/10.1002/oca.709.

[18] Epenoy, R., and Bertrand, R., "Optimal control and smoothing techniques for computing minimum fuel orbital transfers and rendezvous," *18th International Symposium on Space Flight Dynamics (ISSFD)*, Vol. 548, Munich, Germany, 2004, pp. 131–136.

[19] Wang, Y., and Topputo, F., "Indirect optimization of power-limited asteroid rendezvous trajectories," *Journal of Guidance, Control, and Dynamics*, Vol. 45, No. 5, 2022, pp. 131–136. https://doi.org/10.2514/1.G006179.

[20] Wang, Y., and Topputo, F., "Indirect optimization of fuel-optimal many-revolution low-thrust transfers with eclipses," *IEEE Transactions on Aerospace and Electronic Systems*, Vol. 59, No. 1, 2022, pp. 39–51. https://doi.org/10.1109/TAES.2022.3189330.

[21] Epenoy, R., "Fuel optimization of low-thrust trajectories under thrust and coast times constraints: a novel indirect approach," *Acta Astronautica*, Vol. 206, 2023, pp. 218–232. https://doi.org/10.1016/j.actaastro.2023.02.030.

[22] Nurre, N. P., and Taheri, E., "Duty-cycle-aware low-thrust trajectory optimization using embedded homotopy," *Acta Astronautica*, Vol. 212, 2023, pp. 630–642. https://doi.org/10.1016/j.actaastro.2023.08.022.

[23] Mannocchi, A., Giordano, C., and Topputo, F., "A Homotopic Direct Collocation Approach for Operational-Compliant Trajectory Design," *The Journal of the Astronautical Sciences*, 2022, pp. 1–17. https://doi.org/10.1007/s40295-022-00351-x.

[24] Conway, B. A., *Spacecraft trajectory optimization*, Cambridge University Press, Cambridge, UK, 2010. https://doi.org/10.1017/CBO9780511778025.

[25] Longuski, J. M., Guzmán, J. J., and Prussing, J. E., *Optimal control with aerospace applications*, Springer, Berlin, Germany, 2014. https://doi.org/10.1007/978-1-4614-8945-0.

[26] Guo, T., Li, J., Baoyin, H., and Jiang, F., "Pseudospectral Methods for Trajectory Optimization with Interior Point Constraints: Verification and Applications," *IEEE Transactions on Aerospace and Electronic Systems*, Vol. 49, No. 3, 2013, pp. 2005–2017. https://doi.org/10.1109/TAES.2013.6558034.

[27] Russell, R. P., "Primer vector theory applied to global low-thrust trade studies," *Journal of Guidance, Control, and Dynamics*, Vol. 30, No. 2, 2007, pp. 460–472. https://doi.org/10.2514/1.22984.

[28] Zhang, C., Topputo, F., Bernelli-Zazzera, F., and Zhao, Y.-S., "Low-thrust minimum-fuel optimization in the circular restricted three-body problem," *Journal of Guidance, Control, and Dynamics*, Vol. 38, No. 8, 2015, pp. 1501–1510. https://doi.org/10.2514/1.G001080.

[29] Giorgini, J. D., and Yeomans, D. K., "On-line system provides accurate ephemeris and related data," Tech. Rep. NPO-20416, NASA, 1999.